DeforMoBot: A Bio-Inspired Deformable Mobile Robot for Navigation Among Obstacles

Barry William Mulvey, Thilina Dulantha Lalitharatne, and Thrishantha Nanayakkara

***Abstract*—Many animals can move in cluttered environments by conforming their body shape to geometric constraints in their surroundings such as narrow gaps. Most robots are rigid structures and do not possess these capabilities. Navigation around movable or compliant obstacles results in a loss of efficiency—and possible mission failure—compared to progression through them. In this paper, we propose the novel design of a deformable mobile robot; it can adopt a wider stance for greater stability (and possible higher payload capacity), or a narrower stance to become capable of fitting through small gaps and progressing through flexible obstacles. We use a whisker-based feedback control approach in order to match the amount of the robot's deformation with the compliance level of the obstacle. We present a real-time algorithm which uses whisker feedback and performs shape adjustment in uncalibrated environments. The developed robot was tested navigating among obstacles with varying physical properties from different approach angles. Our results highlight the importance of co-development of environment perception and physical reaction capabilities for improved performance of mobile robots in unstructured environments.**

***Index Terms*—biologically-inspired robots, compliant joints and mechanisms, deformable robots, field robots, whisker-based navigation.**

I. Introduction

ROBOTS are increasingly being used as data-gathering platforms in unconventional and unstructured environments [1]. One such example is in nature for habitat monitoring which presents significant challenges in harsh and hostile conditions but is critical to address climate issues [2]. Another is in the monitoring of potentially hazardous settings such as nuclear power stations and oil rigs. There is also growing demand for robots to be employed across a wide range of other unstructured applications involving monitoring, search and rescue, exploration, and so on.

Embodied artificial intelligence proposes that robot bodies and brains are jointly developed in a similar way to the evolution of animals [3]. This concept could allow soft robots to represent bio-inspired artificial intelligence that is not possible with rigid robotics [4], [5]. The ability of a robot to traverse, rather than circumnavigate, obstacles would result in higher efficiency (e.g. less travel time and lower energy expended) and could even be necessary for mission success. Because of the limited power supply which mobile robots possess, it is crucial to choose the most efficient route. However, few solutions have been proposed for this problem, and the topic of progression through obstacles (rather than avoidance of them) is rarely discussed in literature [6].

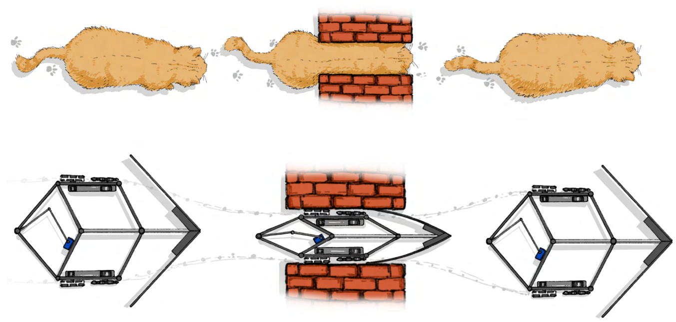

Fig. 1. The ability of animals—such as cats—to morph their shape in order to traverse spaces smaller than their natural body states is the bio-inspiration for the design of our deformable mobile robot.

The motion planning problem of Navigation Among Movable Obstacles (NAMO) enables a robot to analyze its environment and decide whether to manipulate obstacles in its path [7], and has been examined in structured indoor environments [8], [9]. The problem is still open and challenging and its application to more unstructured environments has not yet been adequately explored.

Unwanted obstructions are unavoidable even with near-perfect perception. These undesired collisions have the potential to cause serious damage to a robot and/or its environment. Robust collision detection and physical interaction is important in this context; in the post-impact phase—described in [10]—the robot should detect the collision occurrence and react with a recovery strategy [11]. Animals minimize collision force to reduce risk of injury and damage [12], and introducing similar types of compliance to rigid robots can result in a considerable reduction in the harm that could be inadvertently caused [13].

Given the aforementioned drawbacks in existing approaches and the potential for improvement in this area, we present a novel bio-inspired robot design which utilizes embodied intelligence to traverse obstacles in unstructured environments. Animals such as cats, rats, and cockroaches have the ability to fit through gaps narrower than their resting body shapes. As shown in Fig. 1, cats can readjust their body dimensions through adapting their flexible collarbones, shoulders, and

Manuscript received 9 December 2022; accepted 20 April 2023. This paper was recommended for publication by Editor X. Liu upon evaluation of the Associate Editor and Reviewers' comments. This work was supported in part by the Natural Intelligence for Robotic Monitoring of Habitats through EU Horizon 2020 Research and Innovation Programme under Grant 101016970 and in part by U.K. Engineering and Physical Sciences Research Council (EPSRC) DTP Scholarship jointly with Analog Devices, Inc.

B. W. Mulvey, T. D. Lalitharatne, and T. Nanayakkara are with the Dyson School of Design Engineering, Imperial College London, SW7 2DB, UK. (e-mail: b.mulvey21@imperial.ac.uk).

This paper has supplementary downloadable material available at https://doi.org/10.1109/LRA.2023.3273393, provided by the authors.

Digital Object Identifier (DOI): 10.1109/LRA.2023.3273393.

spines [14], [15]. Their ability to squeeze through spaces narrower than their normal state body dimensions forms the basis of inspiration for our own robot design.

The specific contributions of this paper are

1) The design of a bio-inspired deformable mobile robot (able to alter its shape by applying a force or stress).
2) The development of a haptic-based shape adjustment algorithm in response to proprioceptive feedback in uncalibrated environments, balancing locomotion, stability, and mobility.
3) Real-time estimation of the optimal robot body shape for traversing obstacles with varying compliance and fitting through gaps narrower than its natural width.

The remainder of the paper is organized as follows. Section II discusses relevant related work. Section III presents the methodology, including the design of our robot and its kinematic analysis. Section IV explains the experimentation and also shows the results obtained. Section V discusses our findings and their context in greater detail and also proposes possible areas for future work. Finally, Section VI presents the conclusions of this work.

II. Related Work

Desirable properties of biological organisms—such as adaptivity, robustness, versatility, and agility—can strongly benefit the design of autonomous robots [16]. Over thousands of years, animals have evolved to tune mechanical properties of their bodies to suit the environments they encounter. For mammals such as rats or cats, the ability to squeeze through gaps in a cluttered environment is one of the key adaptations to simplify interactions with their environments [17].

Shape-changing robots have emerged due to technology developments such as deformable soft robotics. Shape change offers opportunities for a robot to enhance or expand its functionality via adaptation. To achieve this, grand challenges to be addressed include enabling shape sensing, automating shape-changing, and integrating functional materials into systems [18].

Reconfiguring its natural shape enables a robot to change its centre of mass. This allows it to be endowed with intrinsic robustness and increased ability to overcome obstacles. It can also assist robots in finding compensatory behaviors in response to damage or injury, at which animals are adept. A trial-and-error learning algorithm was introduced in [19] to conduct experiments that allow robots to rapidly discover a behavior that adapts to damage.

Animals such as cockroaches can crawl rapidly in confined spaces by achieving shape-changing ability through their compliant, soft-bodied exoskeletons which provided inspiration for the development of an origami-style, soft, legged robot that can traverse rapidly in both open and confined spaces [20]. Rolling soft robotics have been inspired by creatures such as spiders, caterpillars, salamanders, and shrimp [21]. One example is GoQBot, a caterpillar-inspired soft-bodied rolling robot, that can switch between crawling and rolling [22]. The octopus has also been used as inspiration for a soft robot capable of underwater pushing-based locomotion and object grasping [23].

Origami robots, also inspired by nature, consist of a combination of folding processes and of smart material actuators. Their elegant designs exhibit soft-body properties and yield compliance [24]. For example, one such miniature origami robot can self-fold, walk, swim, and degrade [25].

The use of inflatable bladders in a soft robot in [26] allowed it to navigate both a flat and an inclined surface better than an equivalent fixed-shape robot. In other work, a simulated soft robot evolved to squeeze its body through a small aperture; an impossible task for a similar rigid-body counterpart [27].

A recently-developed reconfigurable robotic base detailed in [28] allows a fixed-shape robotic platform to better navigate through cluttered environments by using a narrow base, or to carry heavy payloads and to prevent tipping over by using a wide base. A quadrupedal robot has been shown to morphologically adapt to different environmental conditions in unstructured environments [29].

A six-legged, sprawl-tuned autonomous robot (STAR) presented in [30] possesses a variable leg sprawl angle to adapt the robot's stiffness, height, and leg-to-surface contact angle. This allows the miniature robot to move on various terrain surfaces and traverse certain obstacles. These capabilities were built upon and developed further in a reconfigurable rising sprawl-tuned autonomous robot (RSTAR) which can reconfigure the robot's shape and shift the location of its center of mass [6].

Path planning for soft robots in congested environments is a further problem with wide application. An example of a method for squeezing worm-like soft robots in restricted settings is presented in [31], where the calculated optimal path has a trade-off between the size and shape change of the robot and the length of the path. Further inspiration from nature has led to the development of "vine" or growing soft robots to navigate constrained environments [32].

Many of the aforementioned soft robots have limited force capability. Our proposed transformable structure uses rigid-body kinematics to actively change shape based on whisker feedback. Other advantages of our design include the potential to carry payload and additional sensor modalities.

III. Method

A. Design

The design of the robot body with mounted sensors is shown in Fig. 2a with its measurements drawn in Fig. 3a. The hexagonal shape is chosen as it is a naturally-occurring shape known for being robust and strong under compression (e.g. beehive honeycombs, basalt columns, insect eyes) [33], [34]. The addition of three links within the outer shell form two parallelograms and a kite within the hexagon.

A linear guide rail acts as the "spine" of the robot, and spring-loaded "whiskers" are attached to its front tip. An umbrella-inspired mechanism is deployed to result in symmetric movement of the whiskers when either or both of these are impacted. A similar style umbrella-like system attached from the spine to the robot's two front corners ensures symmetry of the body itself when the robot changes shape.

The shape of the robot body—mimicking the transversal contraction of the cat—can change from a regular hexagonal

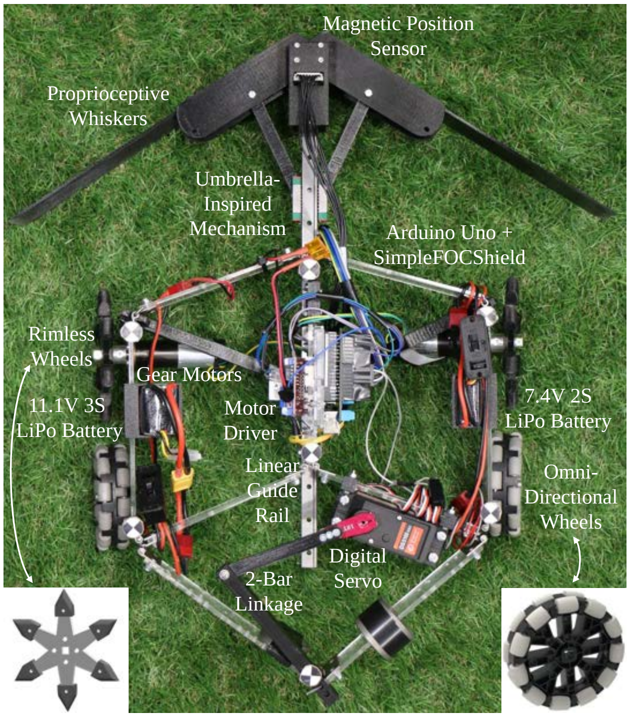

(a)

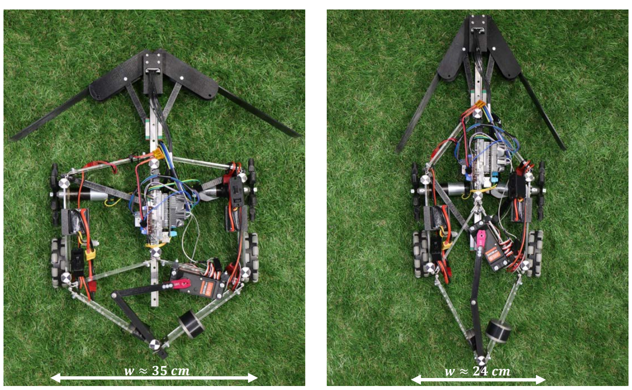

(b) (c)

Fig. 2. (a) Design of the robot body with mounted sensors. Wheels used in the robot design are inset. Inset bottom left: Motor-driven 3D-printed rimless wheels are employed at the front of the robot to provide traction and grip on unstructured terrain. Inset bottom right: Passive omni-directional wheels at the back of the robot are utilized to assist with the robot's shape-changing ability. The body shape can vary between the widest stance shown in (b) to the narrowest stance shown in (c).

shape with width $w \approx 35$ cm (Fig. 2b) to an elongated rhombus shape (Fig. 2c) with $w \approx 24$ cm, approximately 66% of its original width. The robot length changes in the range $47 \text{ cm} \leq l \leq 59$ cm. The length and width of the robot can be written as

$$l = l_1 + l_n + l_1 \cos\frac{\Theta}{2} + l_2 \cos\frac{\Psi}{2} \tag{1}$$

$$w = 2w_{wl} + 2l_1 \sin\frac{\Theta}{2} \tag{2}$$

where l_n is the length of the "neck" part of the robot's spine, w_{wl} is the width of the wheels, and Θ is the angle of deformation of the robot body (influencing the shape of the robot), as shown in Fig. 3a. In our case, with $l_1 \approx 16.5$ cm, $l_2 \approx 13.5$ cm, $w_{wl} \approx 3.5$ cm, and $l_n \approx 17$ cm, we get

$$l = 33.5 + 16.5\cos\frac{\Theta}{2} + 13.5\cos\frac{\Psi}{2} \tag{3}$$

$$w = 7 + 33\sin\frac{\Theta}{2} \tag{4}$$

We show our proposed control block diagram in Fig. 4a. We present a Robot Control Node (RCN) which takes feedback from the Position Measurement and the Shape Controller, and communicates with the Position to Shape Mapper (PSM) and the Motion Controller.

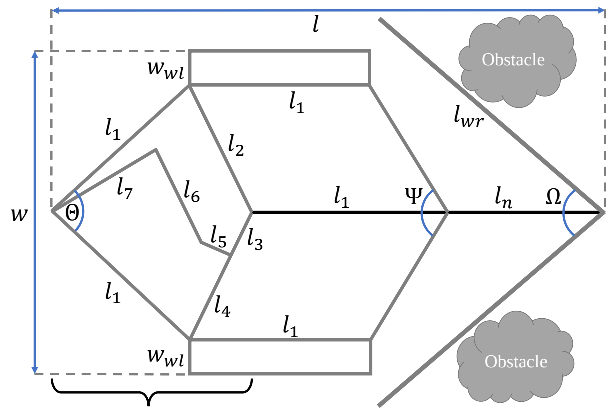

(a)

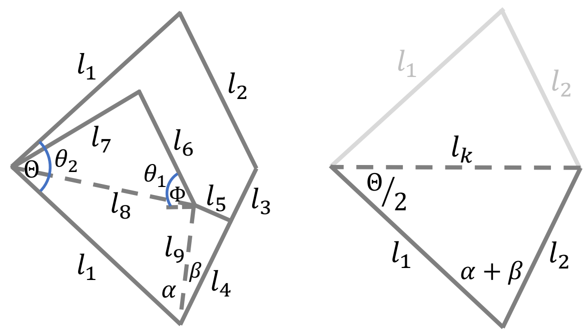

(b) (c)

Fig. 3. (a) Design measurements of the deformable mobile robot as it comes into contact with obstacles. (b) Geometry of the kite section of the robot. (c) Geometry of the bottom half of the kite section of the robot.

B. Materials and Sensors

The robot body is made from sheets of acrylic cut to size. Acrylic is chosen since it is a stable and robust material, while also allowing screw holes to be drilled easily. Screw holes are needed in order to mount different sensors and joints. 38 mm SC 1838 Pattern Steel Butt Hinges are used as the joints of the body. The shell consists of 6 acrylic sheets assembled to form an outer hexagonal shape, with a further 3 acrylic sheets forming parallelograms and a kite within the hexagon. The linear guide rail spine is connected to the middle acrylic piece and spring-loaded 3D-printed whiskers are attached to its front tip. The mass of the full system (including robot body, wheels, motors, and sensors) is approximately 2.5 kg.

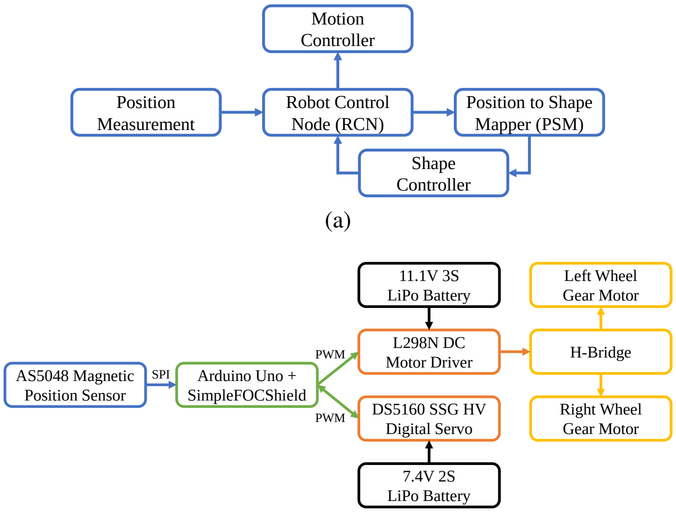

Fig. 4. Control and hardware architecture of the robot. (a) The control block consists of the Position Measurement, Robot Control Node (RCN), Position to Shape Mapper (PSM), Shape Controller, and Motion Controller. (b) The hardware is made up of the controller, sensors, and motors. All measurement analysis and decision-making is performed on the Arduino, while a tethered connection to a laptop is used for data collection.

A block diagram of the hardware used is shown in Fig. 4b. The spring-loaded 3D-printed whiskers are allowed to rotate around a fixed axis, as shown in Fig. 3a. The orientation of a 6mm neodymium magnet attached to these whiskers is measured by an ams OSRAM Adapterboard Development Kit for AS5048A Angle Position. These measurement data (recorded to an accuracy of two decimal places) are sent at a rate of 200 ms to an Arduino Uno mounted with the Simple Field Oriented Control Shield (SimpleFOCShield) v2.0.3. This update rate is faster than the maximum speed of the robot, ensuring quick reaction time to real-time measurements.

We employ two different types of wheels to combine different features, inset in Fig. 2a. The robot's front wheels are 3D-printed rimless wheels which provide traction and grip on unstructured terrain. They are controlled using an L298N DC Motor Driver Module with Arduino, driven by Maxon RE-max 24 Motors with Maxon GP 22 C Planetary Gearheads, and powered by an 11.1V 3S Lithium Polymer (LiPo) battery (Zeee Power). The back wheels are $3.25''$ (260mm Travel) Omni-Directional Anti-Static Wheels (VEX Robotics) which assist with the robot's shape-changing ability.

The robot's body shape is controlled using a DS5160 SSG HV Digital Servo which is powered by a 7.4V 2S Lithium Polymer (LiPo) battery (Zeee Power).

C. Kinematic Analysis

Observing Fig. 3, the servo is placed to enable the greatest range of movement for the 2-bar linkage. For design and geometric simplification, we set the links in the 2-bar linkage to be equal, giving

$$l_6 = l_7 \tag{5}$$

and thus

$$\theta = \theta_1 = \theta_2 \tag{6}$$

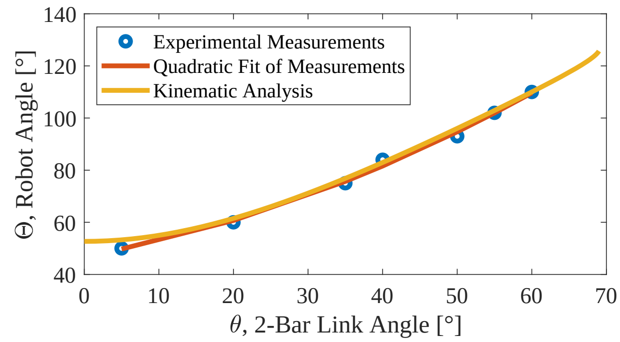

Fig. 5. Validation of the kinematic analysis. The quadratic expression for experimental measurements of Θ (the robot angle) given θ (the 2-bar link angle) is plotted against the kinematic equations derived for same. The overlap of these measurements validates the kinematics analysis presented.

Applying geometric properties to Fig. 3b, we note that

$$l_9 = \sqrt{l_4^2 + l_5^2} \tag{7}$$

$$\beta = \tan^{-1}\frac{l_5}{l_4} \tag{8}$$

Using the law of cosines and with $l_6 = l_7$,

$$l_8 = \sqrt{2l_6^2(1 - \cos(180 - 2\theta))} \tag{9}$$

We also use the law of cosines to find an expression for α since

$$l_8 = \sqrt{l_1^2 + l_9^2 - 2l_1 l_9 \cos\alpha} \tag{10}$$

$$\alpha = \cos^{-1}\frac{l_1^2 + l_9^2 - l_8^2}{2l_1 l_9} \tag{11}$$

Applying geometric properties to Fig. 3c, we equate the kite diagonal l_k as

$$l_k = (l_1 + l_2)\sin\frac{\alpha + \beta}{2} \tag{12}$$

Finally, using the law of sines, we derive an expression for the robot angle Θ as

$$\frac{\sin\frac{\Theta}{2}}{l_2} = \frac{\sin(\alpha + \beta)}{l_k} \tag{13}$$

$$\Theta = 2\sin^{-1}\left(\frac{l_2 \sin(\alpha + \beta)}{l_k}\right) \tag{14}$$

which can be used in (4) to calculate the robot's width.

In our case, we have designed and assembled our robot to have the following measurements: $l_1 \approx 16.5$ cm, $l_2 \approx 13.5$ cm, $l_3 \approx 4.75$ cm, $l_4 \approx 8.75$ cm, $l_5 \approx 2.15$ cm, $l_6 \approx 10.5$ cm, $l_7 \approx 10.5$ cm, $w_{wl} \approx 3.5$ cm, $l_n \approx 17$ cm, and $l_{wr} \approx 26.5$ cm. This means that

$$l_9 = \sqrt{l_4^2 + l_5^2} = \sqrt{8.75^2 + 2.15^2} \approx 9 \text{ cm} \tag{15}$$

$$\beta = \tan^{-1}\frac{l_5}{l_4} = \tan^{-1}\frac{2.15}{8.75} \approx 13.8^\circ \tag{16}$$

Fig. 5 compares the predicted robot angle Θ based on the 2-bar link angle θ from the kinematic equations and the experimental measurements of Θ for different θ values. We measured 7 points, more than the minimum of 4 required

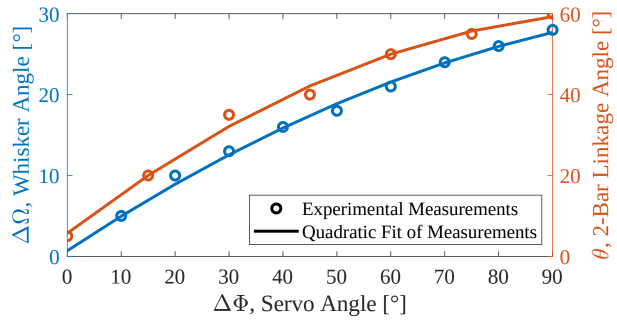

Fig. 6. Comparison of the relationships between the change in servo angle $\Delta\Phi$ and change in whisker angle $\Delta\Phi$ (in blue, left y-axis) and between the change in servo angle $\Delta\Phi$ and 2-bar linkage angle θ (in orange, right y-axis). Both relationships are modelled by quadratic polynomial regression.

to plot the quadratic polynomial model. The overlap of the data plotted in the figure demonstrates a good fit between experimental data and the analytical predictions.

The robot aims to accomplish certain qualitative standards which we can define in linguistic terms as

1) Traverse obstacles in the desired/chosen path.
2) Keep a wide body shape for stability.

Given these objectives, we recall the Position to Shape Mapper (PSM from Fig. 4) and propose the PSM model shown in Fig. 6. The figure shows comparisons of the relationships between the change in the servo angle $\Delta\Phi$ and the change in the whisker angle $\Delta\Omega$ (in blue, left y-axis) and between the change in the servo angle $\Delta\Phi$ and the 2-bar linkage angle θ (in orange, right y-axis). These relationships can be modelled as quadratic polynomials, for example

$$\Delta\Phi = a\Delta\Omega^2 + b\Delta\Omega + c \tag{17}$$

where a, b, and c are hand-tuned coefficients to couple the whisker and desired robot body shape. It is imperative that the tuning of the whisker complements the robot's body shape to elicit meaningful behavior. Overly sensitive whisker perception would lead to an over compensation by the robot when narrowing its body to traverse obstacles, while whisker perception that is too coarse would result in the robot struggling to move through gaps.

To achieve the previously stated objectives, we propose the procedures detailed in Algorithm 1 which the deformable mobile robot can employ to efficiently progress through obstacles. This shape-adjustment algorithm takes account of both the real-time whisker angle deformation and the current shape of the robot body. Traversing obstacles is the robot's primary aim since this makes it as efficient as possible at progressing its locomotion. When the robot experiences little or no obstruction, it adjusts its shape to a wider stance where possible, as optimal stability is its secondary aim.

We have developed this setup to be controllable, meaning that different algorithms can easily be deployed and tested. For example, if the goal is to not disturb the obstacle, the robot can be programmed to fully deform when the whisker senses an angle change.

Algorithm 1 Shape/Mobility Optimization Algorithm

t = current time; t_{th} = threshold time; T = period;
Φ = servo angle; Ω = whisker angle; t_{pass} = elapsed time.
procedure OBSTACLE PROGRESSION(t, t_{th}, T, $\Delta\Omega_t$, $\Delta\Phi_{min}$, $\Delta\Phi_{max}$)
  while $t < T$ **then**
    Drive forwards
    $\Delta\hat{\Phi}_t = a\Delta\Omega_t^2 + b\Delta\Omega_t + c$
    if $\Delta\hat{\Phi}_t > \Delta\Phi_{t-1}$
      $delay = False$
    if $\Delta\hat{\Phi}_t < \Delta\Phi_{t-1}$ **then**
      if $delay = False$ **then**
        $t_{delay} = t$
      $delay = True$
    $t_{pass} = t_{delay} - t$
    if $delay = False$ **or** ($delay$ **and** $t_{pass} \geq t_{th}$)
      if $\Delta\hat{\Phi}_t < \Delta\Phi_{min}$ **then**
        $\Delta\Phi_t = \Delta\Phi_{min}$
      else if $\Delta\hat{\Phi}_t > \Delta\Phi_{max}$ **then**
        $\Delta\Phi_t = \Delta\Phi_{max}$
      else
        $\Delta\Phi_t = \Delta\hat{\Phi}_t$
end procedure

IV. EXPERIMENTS AND RESULTS

We conducted experiments to observe how the robot interacts with obstacles with varied parameters. We used boxes, cushions, clothes, and stone blocks as the obstacles since these cover a range of different physical properties including mass, shape, texture, rigidity/compliance, and hardness/softness.

The obstacles were placed 24 cm apart, the narrowest possible width of the robot. The robot started from a stationary position 20 cm from the edges of the obstacles and travelled at maximum speed for a limited time of 5 seconds to attempt to traverse them. We tested the robot across various approach angles including $90°$ (directly facing the obstacles), $60°$, and $30°$. Smaller angles are more challenging for the robot since the gap is tighter. Based on the compliance of the objects, the robot could push them away (in cases of lighter obstacles), narrow its body to squeeze through the gap (in cases of heavier obstacles), or use a combination of these actions.

The robot obtained the whisker angle measurements (from the magnetic encoder) at an update rate of 200 ms and applied the PSM to change shape (by controlling the servo), adhering to the algorithm detailed in Algorithm 1.

Examples of these experiments are depicted in Fig. 7. Visual markers are placed at different points on the robot to precisely follow its movements and changing body shape through the scene. We track these markers using the Kinovea video annotation tool. In these still images taken from the recorded videos, the robot's path is shown in red to directly compare the transient responses of the robot's body shape and the progression of its path as it traverses the different obstacles at various approach angles.

The robot completed 10 trials attempting to traverse each obstacle from each approach angle (120 trials overall) in the

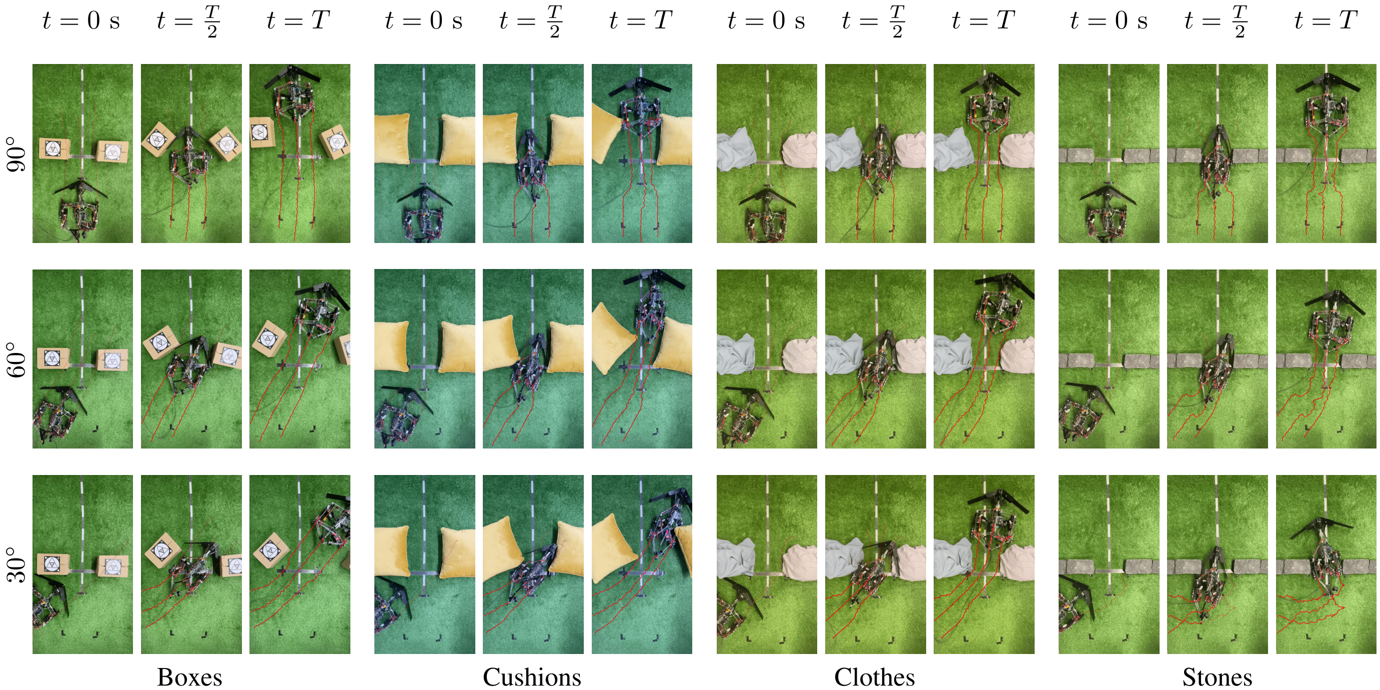

Fig. 7. Comparison of the robot's path (in red) and obstacle displacement following tests involving various obstacles (boxes, cushions, clothes, and stones) as labelled beneath the figure groups. The starting approach angles of the robot are shown in the row headers (to the left of the figures) and the timestamps of the still frames are shown in the column headers (at the top), where $T = 5$ s.

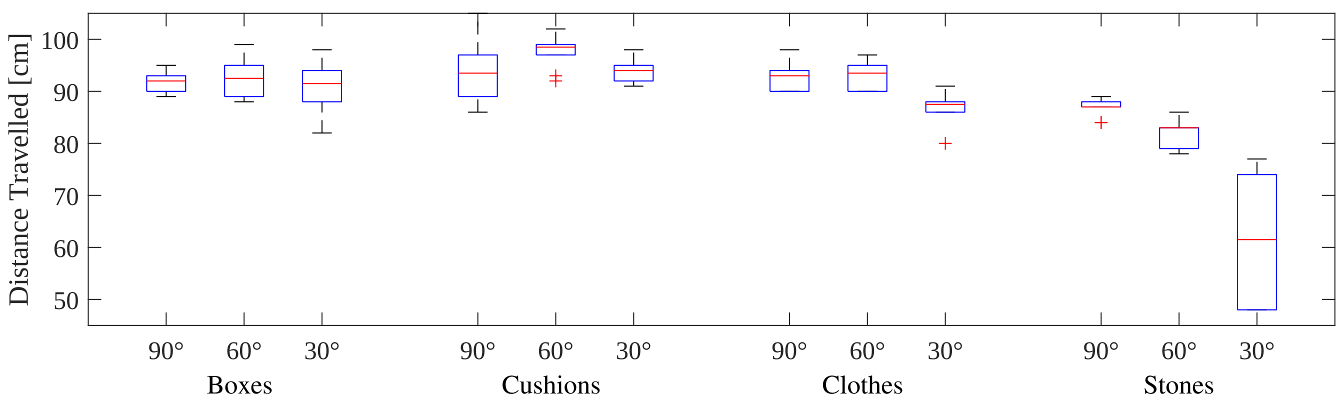

Fig. 8. Box plot of experimental results to visualize summary statistics. Experimental trials involved the robot approaching different obstacles from various starting angles and attempting to traverse them. 10 trials of each scenario was performed and the distance travelled by the robot in 5 seconds was recorded. The plot shows the minimum, lower quartile, median, upper quartile, maximum, and outlier values of each case.

allowed timeframe of 5 seconds. It achieved 100% success rate in 11 of the 12 cases: boxes at approach angles of 90°, 60°, and 30°; cushions at 90°, 60°, and 30°; clothes at 90°, 60°, and 30°; and stone blocks at 90° and 60°. It had a 60% success rate in the other case: stone blocks at 30°. The results are summarized in Fig. 8, where the box plot shows the variance of the distances recorded across the trials.

Fig. 9 shows comparisons of the means of experimental results to demonstrate how the whisker angle and servo angle change during interaction with obstacles in the robot's path. The servo angle is reactive in real-time to data measurements of the whisker angle, apart from a delay when the robot is widening its shape. This delay is included in Algorithm 1 so that the robot only widens its shape once its body has mostly or fully passed through the obstacles.

V. Discussion

Active or passive deformation of the physical body to conform to physical environmental constraints is an elegant capability and example of embodied intelligence shared by many animals such as mice, rats, and cats. Very often these physical reactions are either passive or largely driven solely by haptic perception, especially for animals living in burrows. A lack of such capability and agility often limits mobile robots in unstructured environments. This paper examines a robot that can adapt to its environment, much like animals, and perform a transversal collapse of its body in response to proprioceptive feedback from a symmetrical whisker. We conducted experiments for gaps narrower than the robot's body for different approach angles and different types of the

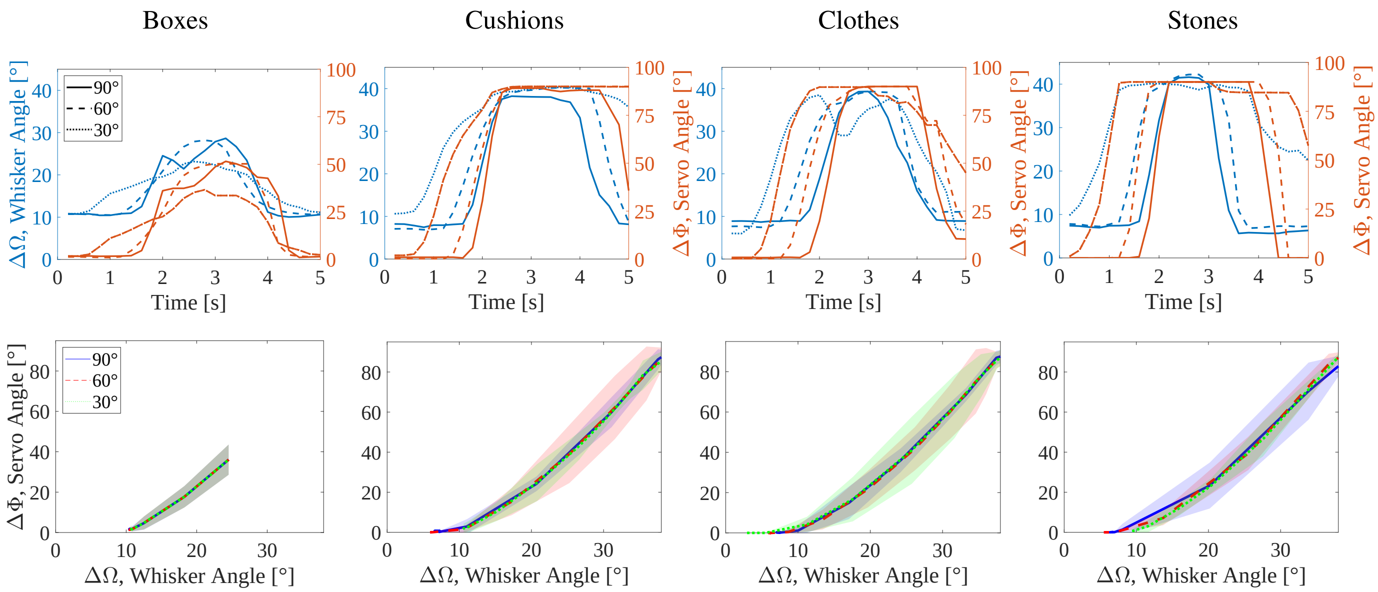

Fig. 9. Comparison of how the whisker angle and servo angle change during interaction with various obstacles from different approach angles. The obstacles are named in the column headers while the approach angles are detailed in the legend of the leftmost figure for each row. Top Row: The servo angle (in orange, right y-axes) is reactive in real-time to data measurements of the whisker angle (in blue, left y-axes) with an in-built delay in the case of the robot widening its shape (to allow the robot to progress its body through the obstacle and avoid becoming trapped). Bottom Row: Direct comparison of the angles relationship where the mean is plotted surrounded by standard deviation shading.

obstacles.

Our results show the importance of tuning haptic perception to match the physical capabilities of the robot. Observing Fig. 7, we note that when the robot can push away lighter obstacles such as boxes, it only slightly adjusts its body shape. For more moderately-weighted obstacles such as cushions and clothes, the robot cannot move the obstruction as much and so adjusts it body shape accordingly. When the robot cannot move or push the obstacles at all (as with the stones), it completely relies on adjusting its configuration until it has successfully traversed the obstacle at which time it can resume its natural body shape.

This is further confirmed by box plots of distance travelled within 5 seconds as shown in Fig. 8. The robot achieves 100% success rate in 11 of 12 cases—traversing boxes, cushions, and clothes at all approach angles of 90°, 60°, and 30°, and stones at 90° and 60°—with little deviation in the distance covered. In the single remaining case (immovable stones at 30°), it achieves 60% success rate with greater deviation in the distance covered. Given a longer timeframe, the robot may have been more successful in this particular case.

Further examining the top row of plots in Fig. 9, there are steeper gradients when heavier obstacles are used, resulting in a quicker angle change to the whisker. A direct comparison between the change in the whisker angle Ω and the change in the servo angle Φ for each obstacle is shown in the bottom row of plots in Fig. 9. Only measurements before angle decreases are shown so that the incorporated "widening delay" does not distort the comparison. The mean is plotted surrounded by standard deviation shading. As expected, the plots show the quadratic relationship between whisker and servo angles.

By narrowing its shape, the robot elongates which may affect its turning capabilities in confined environments. The lack of haptic sensing at the back of the robot could potentially reduce its adaptability in such a scenario. However, we have observed that the robot has a smaller turning radius and is able to use its longer, narrower shape to jostle through challenging apertures when approaching at acute angles. The long whiskers help the robot to turn and also protect the robot's body and wheels.

The capability of the robot to employ a wider or a narrower body shape could also help with navigating different terrain types. Animals such as cats are adept on unstructured surfaces due to their flexible vertebrae (assisting with flexion and torsion), and this can inspire future work on the investigation of passive joints or links with multiple degrees of freedom to provide a more flexible spine. Otherwise, employing different types of wheels could potentially help in these scenarios.

When the robot must squeeze through obstacles, it can be upheld by the obstacles themselves. Conversely, pushing lighter obstacles out of the way—instead of deforming its body shape every time it encounters obstacles—allows the robot to maintain its stability.

These capabilities will facilitate improved perception and proficiency of robots resulting in their ability to navigate efficiently and effectively, particularly in unstructured environments, hazardous settings, and challenging terrain.

In future work, it will be interesting to explore the marginal gains of adding more degrees of freedom for deformation and more sensing modalities for predictive and adaptive navigation in unstructured environments.

VI. Conclusions

This work details the design of a novel bio-inspired deformable mobile robot. By enabling the robot to analyze its surroundings, identify obstacles in its path, and adapt its body shape, it can successfully traverse obstacles rather than having to circumnavigate them. This shape adaptation allows it to compress its shape to approximately 66% and to fit through gaps smaller than its natural shape. Our results highlight that the robot's capability to interpret whisker feedback relative to its physical narrowing capability led to meaningful obstacle negotiation behaviors. This is achieved through the integration of a real-time shape adjustment algorithm which takes account of the robot's current shape and the proprioceptive whisker feedback which it receives. Further, we present the results from experiments involving the robot attempting to traverse obstacles with varying physical properties: boxes, cushions, clothes, and stones. These obstacles were placed apart at a distance smaller than the robot's natural width and the robot approached them from various angles. Given a limited time allowed for traversal, the robot achieved 100% success rate in 11 of the 12 cases tested, and 60% success rate in the remaining case. In general, our results highlight the importance of co-development of environment perception and physical reaction capabilities for better performance of mobile robots in unstructured environments.

References

[1] M. Dunbabin and L. Marques, "Robots for environmental monitoring: Significant advancements and applications," *IEEE Robotics & Automation Magazine*, vol. 19, no. 1, pp. 24–39, 2012.

[2] European Union, "Natural Intelligence for Robotic Monitoring of Habitats," 2021. [Online]. Available: https://cordis.europa.eu/project/id/101016970

[3] R. Pfeifer and J. Bongard, *How the body shapes the way we think: a new view of intelligence*. MIT Press, 2006.

[4] S. Kim, C. Laschi, and B. Trimmer, "Soft robotics: a bioinspired evolution in robotics," *Trends in Biotechnology*, vol. 31, no. 5, pp. 287–294, 2013.

[5] D. Rus and M. T. Tolley, "Design, fabrication and control of soft robots," *Nature*, vol. 521, no. 7553, pp. 467–475, 2015.

[6] L. Yehezkel, S. Berman, and D. Zarrouk, "Overcoming obstacles with a reconfigurable robot using reinforcement learning," *IEEE Access*, vol. 8, pp. 217 541–217 553, 2020.

[7] M. Stilman and J. J. Kuffner, "Navigation among movable obstacles: Real-time reasoning in complex environments," *International Journal of Humanoid Robotics*, vol. 2, no. 04, pp. 479–503, 2005.

[8] M. Wang, R. Luo, A. Ö. Önol, and T. Padir, "Affordance-based mobile robot navigation among movable obstacles," in *2020 IEEE/RSJ International Conference on Intelligent Robots and Systems (IROS)*. IEEE, 2020, pp. 2734–2740.

[9] K. Ellis, H. Zhang, D. Stoyanov, and D. Kanoulas, "Navigation among movable obstacles with object localization using photorealistic simulation," in *2022 IEEE/RSJ International Conference on Intelligent Robots and Systems (IROS)*. IEEE, 2022.

[10] A. De Luca, A. Albu-Schaffer, S. Haddadin, and G. Hirzinger, "Collision detection and safe reaction with the DLR-III lightweight manipulator arm," in *2006 IEEE/RSJ International Conference on Intelligent Robots and Systems*. IEEE, 2006, pp. 1623–1630.

[11] S. Haddadin, A. Albu-Schaffer, A. De Luca, and G. Hirzinger, "Collision detection and reaction: A contribution to safe physical human-robot interaction," in *2008 IEEE/RSJ International Conference on Intelligent Robots and Systems*. IEEE, 2008, pp. 3356–3363.

[12] Y. Blum, H. R. Vejdani, A. V. Birn-Jeffery, C. M. Hubicki, J. W. Hurst, and M. A. Daley, "Swing-leg trajectory of running guinea fowl suggests task-level priority of force regulation rather than disturbance rejection," *PloS one*, vol. 9, no. 6, p. e100399, 2014.

[13] A. Albu-Schaffer, O. Eiberger, M. Grebenstein, S. Haddadin, C. Ott, T. Wimbock, S. Wolf, and G. Hirzinger, "Soft robotics," *IEEE Robotics & Automation Magazine*, vol. 15, no. 3, pp. 20–30, 2008.

[14] F. Richmond and D. Bakker, "Anatomical organization and sensory receptor content of soft tissues surrounding upper cervical vertebrae in the cat." *Journal of Neurophysiology*, vol. 48, no. 1, pp. 49–61, 1982.

[15] R. A. Russell, "Using tactile whiskers to measure surface contours," in *Proceedings 1992 IEEE International Conference on Robotics and Automation*. IEEE Computer Society, 1992, pp. 1295–1296.

[16] R. Pfeifer, M. Lungarella, and F. Iida, "Self-organization, embodiment, and biologically inspired robotics," *Science*, vol. 318, no. 5853, pp. 1088–1093, 2007.

[17] M. H. Dickinson, C. T. Farley, R. J. Full, M. Koehl, R. Kram, and S. Lehman, "How animals move: an integrative view," *Science*, vol. 288, no. 5463, pp. 100–106, 2000.

[18] D. Shah, B. Yang, S. Kriegman, M. Levin, J. Bongard, and R. Kramer-Bottiglio, "Shape changing robots: bioinspiration, simulation, and physical realization," *Advanced Materials*, vol. 33, no. 19, p. 2002882, 2021.

[19] A. Cully, J. Clune, D. Tarapore, and J.-B. Mouret, "Robots that can adapt like animals," *Nature*, vol. 521, no. 7553, pp. 503–507, 2015.

[20] K. Jayaram and R. J. Full, "Cockroaches traverse crevices, crawl rapidly in confined spaces, and inspire a soft, legged robot," *Proceedings of the National Academy of Sciences*, vol. 113, no. 8, pp. E950–E957, 2016.

[21] R. H. Armour and J. F. Vincent, "Rolling in nature and robotics: A review," *Journal of Bionic Engineering*, vol. 3, no. 4, pp. 195–208, 2006.

[22] H.-T. Lin, G. G. Leisk, and B. Trimmer, "GoQBot: a caterpillar-inspired soft-bodied rolling robot," *Bioinspiration & Biomimetics*, vol. 6, no. 2, p. 026007, 2011.

[23] M. Calisti, M. Giorelli, G. Levy, B. Mazzolai, B. Hochner, C. Laschi, and P. Dario, "An octopus-bioinspired solution to movement and manipulation for soft robots," *Bioinspiration & biomimetics*, vol. 6, no. 3, p. 036002, 2011.

[24] D. Rus and M. T. Tolley, "Design, fabrication and control of origami robots," *Nature Reviews Materials*, vol. 3, no. 6, pp. 101–112, 2018.

[25] S. Miyashita, S. Guitron, M. Ludersdorfer, C. R. Sung, and D. Rus, "An untethered miniature origami robot that self-folds, walks, swims, and degrades," in *2015 IEEE International Conference on Robotics and Automation (ICRA)*. IEEE, 2015, pp. 1490–1496.

[26] D. S. Shah, J. P. Powers, L. G. Tilton, S. Kriegman, J. Bongard, and R. Kramer-Bottiglio, "A soft robot that adapts to environments through shape change," *Nature Machine Intelligence*, vol. 3, no. 1, pp. 51–59, 2021.

[27] N. Cheney, J. Bongard, and H. Lipson, "Evolving soft robots in tight spaces," in *Proceedings of the 2015 Annual Conference on Genetic and Evolutionary Computation*, 2015, pp. 935–942.

[28] J. Pankert, G. Valsecchi, D. Baret, J. Zehnder, L. L. Pietrasik, M. Bjelonic, and M. Hutter, "Design and motion planning for a reconfigurable robotic base," *IEEE Robotics and Automation Letters*, vol. 7, no. 4, pp. 9012–9019, 2022.

[29] T. F. Nygaard, C. P. Martin, J. Torresen, K. Glette, and D. Howard, "Real-world embodied AI through a morphologically adaptive quadruped robot," *Nature Machine Intelligence*, vol. 3, no. 5, pp. 410–419, 2021.

[30] D. Zarrouk, A. Pullin, N. Kohut, and R. S. Fearing, "STAR, a sprawl tuned autonomous robot," in *2013 IEEE International Conference on Robotics and Automation*. IEEE, 2013, pp. 20–25.

[31] E. Gough, A. T. Conn, and J. Rossiter, "Planning for a tight squeeze: Navigation of morphing soft robots in congested environments," *IEEE Robotics and Automation Letters*, vol. 6, no. 3, pp. 4752–4757, 2021.

[32] E. W. Hawkes, L. H. Blumenschein, J. D. Greer, and A. M. Okamura, "A soft robot that navigates its environment through growth," *Science Robotics*, vol. 2, no. 8, p. eaan3028, 2017.

[33] A. Bejan, *Shape and structure, from engineering to nature*. Cambridge University Press, 2000.

[34] Q. Zhang, X. Yang, P. Li, G. Huang, S. Feng, C. Shen, B. Han, X. Zhang, F. Jin, F. Xu *et al.*, "Bioinspired engineering of honeycomb structure–using nature to inspire human innovation," *Progress in Materials Science*, vol. 74, pp. 332–400, 2015.